ELSEVIER

NeuroImage

www.elsevier.com/locate/ynimg
NeuroImage xx (2004) xxx–xxx

A myelo-architectonic method for the structural classification of cortical areas

J. Annese,[a,b] A. Pitiot,[a,c] I.D. Dinov,[a,d] and A.W. Toga[a,*]

[a] *Laboratory of Neuro Imaging, Department of Neurology, UCLA School of Medicine, Los Angeles, CA 90095-1769, USA*
[b] *Center for Cognitive Neuroscience, Dartmouth College, Hanover, NH 03755, USA*
[c] *EPIDAURE Laboratory, INRIA, Sophia Antipolis, Cedex 06902, France*
[d] *Department of Statistics, UCLA, Los Angeles, USA*

Received 17 December 2002; revised 11 July 2003; accepted 14 August 2003

We describe an automatic and reproducible method to analyze the histological design of the cerebral cortex as applied to brain sections stained to reveal myelinated fibers. The technique provides an evaluation of the distribution of myelination across the width of the cortical mantle in accordance with a model of its curvature and its intrinsic geometry. The profile lines along which the density of staining is measured are generated from the solution of a partial differential equation (PDE) that models the intermediate layers of the cortex. Cortical profiles are classified according to significant components that emerge from wavelet analysis. Intensity profiles belonging to each distinct class are normalized and averaged to produce area-specific templates of cortical myelo-architecture.

Keywords: Myelo-architecture; Cerebral cortex; Cortical areas

Introduction

The extensive application of MR imaging techniques with submillimetric spatial resolution has revived interest in a topographically organized description of the human cortex that transcends images of superficial lobar or sulcal patterns. There are encouraging indications that microscopic cortical anatomy could be acquired through MR noninvasive imaging of the brain (Clark, 1992; Barbier et al., 2002). However, at present, the internal structure of the cortex is examined chiefly through histological analysis of post-mortem specimens (Annese and Toga, 2002). In this respect there has been recent reprisal of classical architectonic investigations (e.g., Annese and Toga, 2002; Roland et al., 1997; Zilles et al., 2002).

Early work demonstrated that the cortical mantle is not a uniform layer of gray matter, but that it is striped by a distinct internal lamination (Baillarger, 1840; Gennari, 1782; Vicq d'Azyr, 1786). Moreover, such stratified structural design was shown to vary locally on the surface of the hemispheres (Bevan-Lewis, 1878; Meynert, 1872). In fact, systematic histological surveys of the cortical surface culminated in very complex parcellation schemes (Brodmann, 1909; Campbell, 1905; Elliot Smith, 1907; Vogt and Vogt, 1919; von Economo and Koskinas, 1925). Two principal histological features, complementary to a certain extent, have shaped classical maps of the human cortex: the size and distribution of neuronal cell bodies and the density and arrangement of myelinated fibers across the depth of the cortex. These patterns are studied histologically at low power magnification in cross sections of the cortex. It is these features that, following specific staining techniques, make the cortex appear unquestionably and ubiquitously laminated (see Figs. 1A and B).

The density of staining in each layer of the cortex can be recorded by algorithms that measure pixel intensity values along cross-sectional lines (traverses) drawn manually (Zilles and Schleicher, 1993) or semiautomatically (Schleicher et al., 1999) from the pial surface to the white matter border. This approach derives from the original photometric studies of cortical myelination by Hopf (1965) in which each cortical region was characterized by the shape of locally sampled intensity profiles.

A crucial issue in the implementation of an observer-independent and automatic architectonic analysis is the outline of the traverses across the cortex, that is, the paths along which pixel intensities will be measured. The cortical ribbon is not homogeneous internally but presents a complex radial and tangential internal structural framework. The effect of curvature on the internal structure of the cortex was predicted by Bok (1959) on theoretical grounds and studied empirically by Smart and McSherry (1986a,b) in the developing brain of the ferret (Mustelidae). Bok (1959) subdivided the cortical volume into a regular grid of constant dimensions, Smart and McSherry (1986b) drew their cortical grid by tracing the intersection of horizontal laminae with radial lines that followed glial fibers and cellular columns. Both studies indicated that the cortical layers are subject to considerable geometrical distortion during gyrogenesis as indicated by the change in the curvature and direction of

* Corresponding author. Laboratory of Neuro Imaging, Department of Neurology, UCLA School of Medicine, Room 4-238, 710 Westwood Plaza, Box 951769, Los Angeles, CA 90095-1769. Fax: +1-310-206-5518.
E-mail address: toga@loni.ucla.edu (A.W. Toga).
Available online on ScienceDirect (www.sciencedirect.com.)

1053-8119/$ - see front matter © 2003 Elsevier Inc. All rights reserved.
doi:10.1016/j.neuroimage.2003.08.024

radial lines. These studies suggest that a model of the internal structure of the cortex is necessary to generate correct intensity profiles and hence to obtain a meaningful characterization of architectonic areas. In fact, if the transverses are not consistently perpendicular to the cortical layers, or if they intersect, the resulting intensity profiles will be distorted and will contain high levels of noise.

To model the curvature of intracortical layers, we adopted the heat conduction differential equation that Jones et al. (Jones et al., 2000) applied to MRI brain volumes to measure cortical thickness. In our case, working with 2-D histological images, the solution of the Laplace equation generates a series of nested equipotential contours (*n* intermediate cortical layers) between the pial surface and the gray and white matter border. This computational framework produces correct field lines along which the density of staining can be measured. These lines satisfy two important conditions: they do not intersect and they are orthogonal to each inner cortical layer.

Cortical architectonic parcellation requires the definition a priori of the structural elements that will provide anatomical information and that will gauge the comparison between different areas. Our classification is based on architectonic features of myelination: those structural patterns produced by intracortical fiber systems. In this respect, myelin staining reveals evident local structural variations in the cortex produced by changes in both the laminar and radial disposition of fibers. Horizontal and vertical fiber bundles can be arranged in several different ways across the width of the cortex. In fact, one limitation of classical and customary studies of cortical architecture is that the discrimination between these structural patterns has been subjective or based on very complex and arbitrary schemes of interpretation (Vogt, 1910).

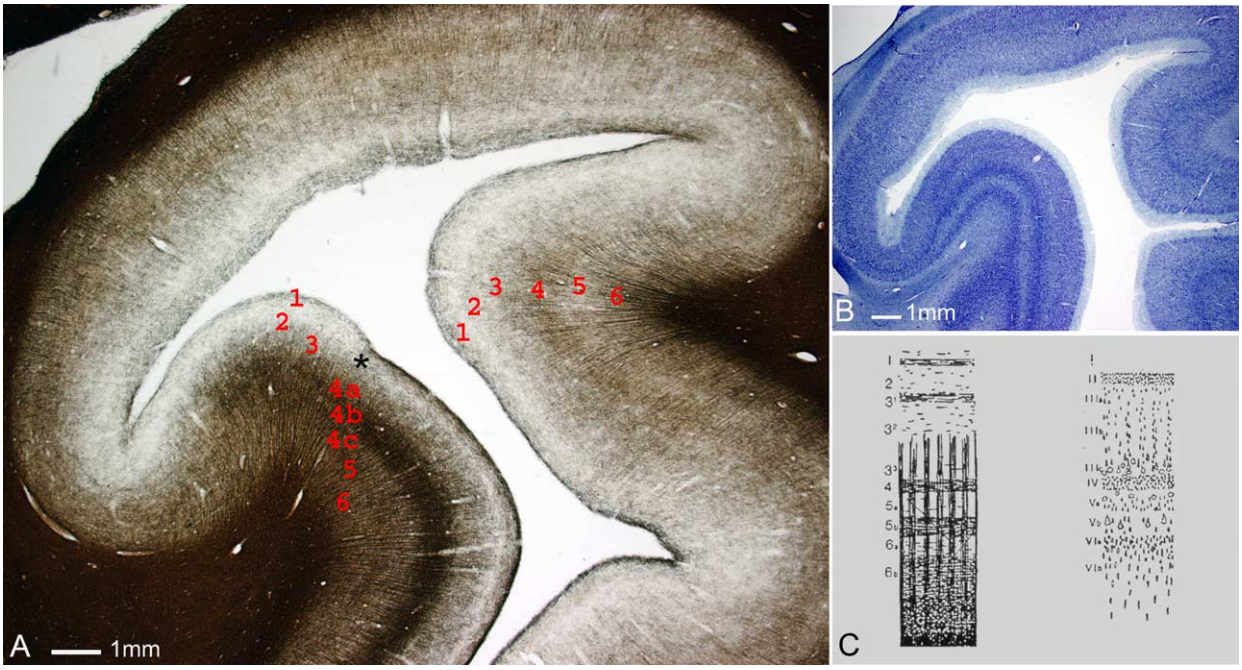

Fig. 1. Cross-sectional images of the cortex at comparable locations in the calcarine sulcus. The limit (*) of the striate cortex (V1) is evident in both the myelin (A) and Nissl (B) preparations. (C) Represents the schematic diagram from Vogt (1910) that reconciles schemes of *myelo*-architectural and *cyto*-architectural lamination in the cortex. This laminar subdivision reflects classical attempts to conform to the homogenetic six-layered lamination proposed by Brodmann (1909) for Nissl-stained material. With respect to myelo-architecture, the cortex is customarily subdivided in the following layers: *Layer 1* is almost exclusively occupied by tangential fibers that convey cortico-cortical feedback input. Long-range dendrites of Cajal–Retzius cells reside in this stratum and can travel for several millimeters. This layer can be considered to be the basis of integration across multiple receptive fields of neurons situated in layers below. *Layer 2* is the poorest in horizontal fibers, Vogt and Vogt (1919) named this layer dysfibrous. However, there are fibers in this layer and they are predominantly radial, running that is, perpendicular and towards the cortical surface. Apical dendrites of most classes of pyramidal neurons, generally the larger sized, can be found in this layer. It should be mentioned that in selected cortical regions (notably in the auditory region) there is a manifest horizontal fiber bundle. This line is usually called the stripe of Kaes–Bechterew created mainly by apical dendrite collaterals of pyramidal cells in layer V. *Layer 3* shows a gradient of myelination that corresponds to the gradient of pyramidal neurons that are typical of this layer, the largest pyramidals being closer to the border with the underlying layer IV. It is harder to discretize this layer into three subdivisions based on gradient of fiber density than it is based on the gradient of neuronal cell bodies. *Layer 4* hosts the external stripe of Baillarger (1840) as its predominant feature (in Nissl-stained material this is the granular layer). Like Layer 1, the fibers in layer 4 are for the most part tangential. The conspicuous collection of horizontal fibers is composed of collaterals of afferent thalamic fibers that make connection with granule cells. There is also a variable density of intracortical association fibers. *Layer 5* (ganglionic layer V), like layer 3, may show a gradient of myelination both in terms of radial and horizontal fibers, because it also presents, from a *cyto*-architectonic view, a vertically graded population of pyramidal neurons of different perikaral size. The deepest portion of layer 5 hosts a second evident continuous bundle of horizontal fibers, which is the innermost stripe Baillarger had reported originally (Baillarger, 1840). *Layer 6* is crowded with both horizontal and radial fibers, the former being, for the major part, a collection of collaterals of the efferent axonal subpopulation of the latter. In the concave floor of sulci, one can however clearly distinguish arcuate association fibers that connect adjacent gyri.

An independent algorithm for the unsupervised classification of myelo-architectonic types would need to be instructed on what to look for along the cortical ribbon. A basic target could be the six-layered isocortical scheme, with two main horizontal bands (Vogt, 1910; see Fig. 1C); the profile arrays produced from each sample would then be classified according to their similarity to the target. In this case, the architectonic classification would be driven by a strong initial hypothesis on cortical structure. However, since cortical myelo-architecture shows extreme—and not well documented—variations, we did not gauge our classification with respect to a single basic architecture. Instead, we propose an automated scheme to assess profile similarity based on significant components derived from wavelet analysis.

Mapping the topography of cortical areas and thus understanding the relationship between structure and function in the cerebral cortex are both a classification and a localization problem. The definition of unambiguous architectonic templates is the prerequisite for topographic histological surveys and hence for comparative studies and for the generalization of architectonic maps to a population. Therefore, we compute averages of profiles that belong to the same class in order to construct synthetic structural models that are easily recognizable and that can be localized topographically on the cortical mantle.

Materials and methods

Preparation of histological material

The material presented in this publication has been sampled from whole serial sections (n = 20) belonging to four different human brain specimens. Specimens were removed from the skull and fixed by immersion in 4% phosphate-buffered paraformaldehyde. The tissue was embedded, but not infiltrated in 7% gelatin creating a coating thick enough (0.5–1 cm) to minimize distortion of the gyri and to hold in place parts of the section that would otherwise naturally dissociate.

Specimens were cut frozen on a Jung Tetrander manual sliding microtome (Jung, Heidelberg) at an interval of 50 μm. Sections were stored free floating in phosphate-buffered solution at 4 °C before being stained.

We stained sections according to a silver impregnation technique modified from Gallyas (1979). The procedure consists of an initial acetylation process followed by four main subsequent steps. The tissue is immersed in a weak solution of ammoniacal silver nitrate. During impregnation, if the solution is maintained within a limited pH range, myelin specifically reduces the silver to its colloidal form. The production of metallic silver by other tissue elements is suppressed by the prior acetylation procedure. The deposition of silver particles on any myelinated fiber, even of very small caliber, occurs at this stage. Physical development follows the impregnation step. Silver in the developer solution is attracted to reduced silver particles on the myelin sheath building up the deposition of black metallic silver to levels that are detectable microscopically. A third differentiation step is run to bleach out excessive deposition of silver. This step maximizes the contrast of the fine pattern of myelination within the cortical mantle against background staining.

Sections were finally dehydrated and cleared in xylene before being sealed in between large format glass slides and covers.

Digital imaging

Whole stained sections were digitized on an Agfa Duoscan flat bed scanner (Agfa, Ridgfield Park, NJ) by a transparent attachment intended for transmitted light scanning. These images were used to trace the reference contours of the section, that is, the pial surface of the mantle and the border between the white matter and gray matter. This level of resolution (1 pixel = 40 μm) enables the determination of local variations in staining intensity, and the disposition of horizontal fiber bundles.

Images at higher magnification were sampled from the sections and captured with a Nikon DX1200 digital camera (Nikon, USA), mounted on an Olympus AX70 research microscope (Olympus, USA). The microscope is equipped with a macro condenser and lens (0.5×) for low power magnification over a relatively large field of view (53 mm). Microscope images contain 3000 × 4000 pixels (resolution: 15 μm/pixel).

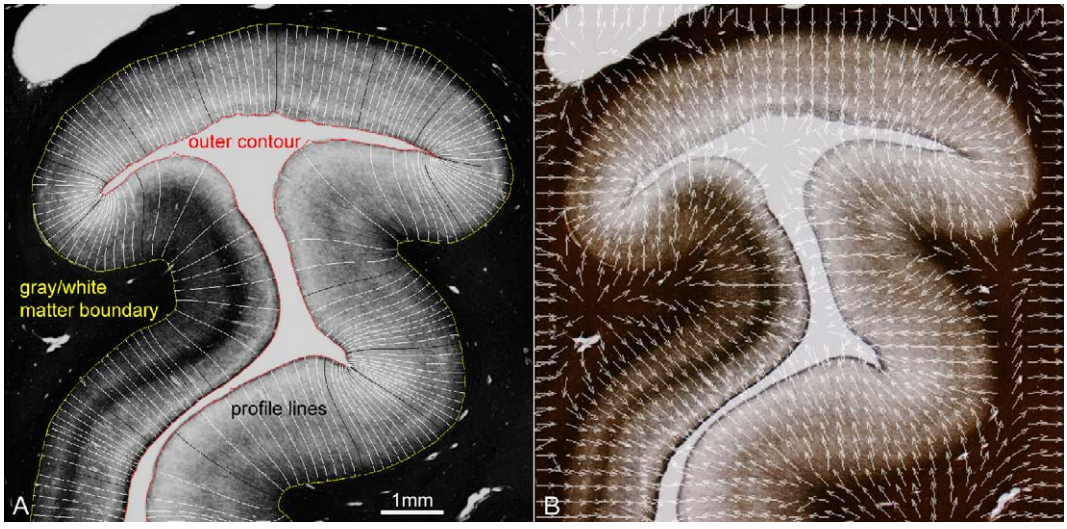

Fig. 2. (A) A sample of cortical traverses (black and white lines) derived from the gradient field computed between the pial surface (red) and the white matter–gray matter border (yellow). (B) Gradient field (blue arrows) computed from the solution of the heat conduction equation (grayscale image).

Cortical profile modeling

For each histological section, we first manually delineate the reference contours. We then solve, using a finite difference scheme, the classical heat conduction equation $\partial u/\partial t = \Delta u$ with the Dirichlet boundary condition: $u = u_1 \in \mathbb{R}$ on the pial contour and $u = u_2 < u_1$ on the cortex–white matter border.

More precisely, we superimpose on the rasterized histological section image a regular computational grid or lattice whose sites correspond to an integer subdivision of the image pixels (a super-sampling of the image). We then use a forward-time, centered-space, finite-difference approximation to compute a numerical solution to our heat conduction equation.

$$\frac{\partial u}{\partial t} = \Delta u \Leftrightarrow \frac{\partial u}{\partial t} = \frac{\partial^2 u}{\partial x^2} + \frac{\partial^2 u}{\partial y^2}$$

becomes

$$\frac{u_{i,j}^{t+1} - u_{i,j}^{t}}{\mathrm{d}t} = \frac{u_{i+1,j}^{t} - 2u_{i,j}^{t} + u_{i-1,j}^{t}}{\mathrm{d}x^2} + \frac{u_{i,j+1}^{t} - 2u_{i,j}^{t} + u_{i,j-1}^{t}}{\mathrm{d}y^2}$$

where $u_{i,j}^{t}$ is the approximation of the value of the field u at time step $t.\mathrm{d}t$ at position $(i\mathrm{d}x, j\mathrm{d}y)$ with $\mathrm{d}x$, $\mathrm{d}y$ the lattice step sizes in both direction (i.e., the sizes of the pixels in the super-sampled rasterized histological section).

By rearranging our finite-difference approximation, we get:

$$u_{i,j}^{t+1} = \frac{\mathrm{d}t}{\mathrm{d}x^2}\left(u_{i+1,j}^{t} + u_{i-1,j}^{t}\right) + \frac{\mathrm{d}t}{\mathrm{d}y^2}\left(u_{i,j+1}^{t} + u_{i,j-1}^{t}\right) + \left(1 - \frac{2\mathrm{d}t}{\mathrm{d}x^2} - \frac{2\mathrm{d}t}{\mathrm{d}y^2}\right)u_{i,j}^{t}$$

which tells us how to compute $u_{i,j}^{t+1}$ from the values of u^t on a cross-shaped stencil defined around $(i\mathrm{d}x, j\mathrm{d}y)$.

u is first initialized at u_1 and u_2 on the pial contour and cortex–white matter border, respectively. We then iteratively apply the above discrete scheme until convergence. To avoid instability, we choose a $\mathrm{d}t$ that satisfies the Courant condition:

$$\mathrm{d}t \leqslant \frac{1}{2\left(\frac{1}{\mathrm{d}x^2} + \frac{1}{\mathrm{d}y^2}\right)}.$$

Once the partial differential equation (PDE) has converged ($\Delta u = 0$), the gradient of the resulting potential field enables us to compute field lines between the two contours. For every point along the pial contour, we integrate the normalized gradient of the potential field: $N = -(\nabla u/\|\nabla u\|)$ using a classic finite difference approximation for the gradient:

$$\nabla u = \left[\frac{\partial u}{\partial x}\ \frac{\partial u}{\partial y}\right]^T$$

becomes

$$\left[\frac{u_{i+1,j}^{t} - u_{i-1,j}^{t}}{2\mathrm{d}x}\ \frac{u_{i,j+1}^{t} - u_{i,j-1}^{t}}{2\mathrm{d}y}\right]^T$$

In essence, for each point, we follow a path orthogonal to the isopotential lines of u, and record along the way the intensity of the histological section at the visited pixels, until we reach the cortex–white matter border.

Given that the solution to our PDE is a harmonic function, those field lines have the following desirable properties:

- They do not intersect or self-intersect.
- They are nominally parallel.
- They reach both contours at a right angle.

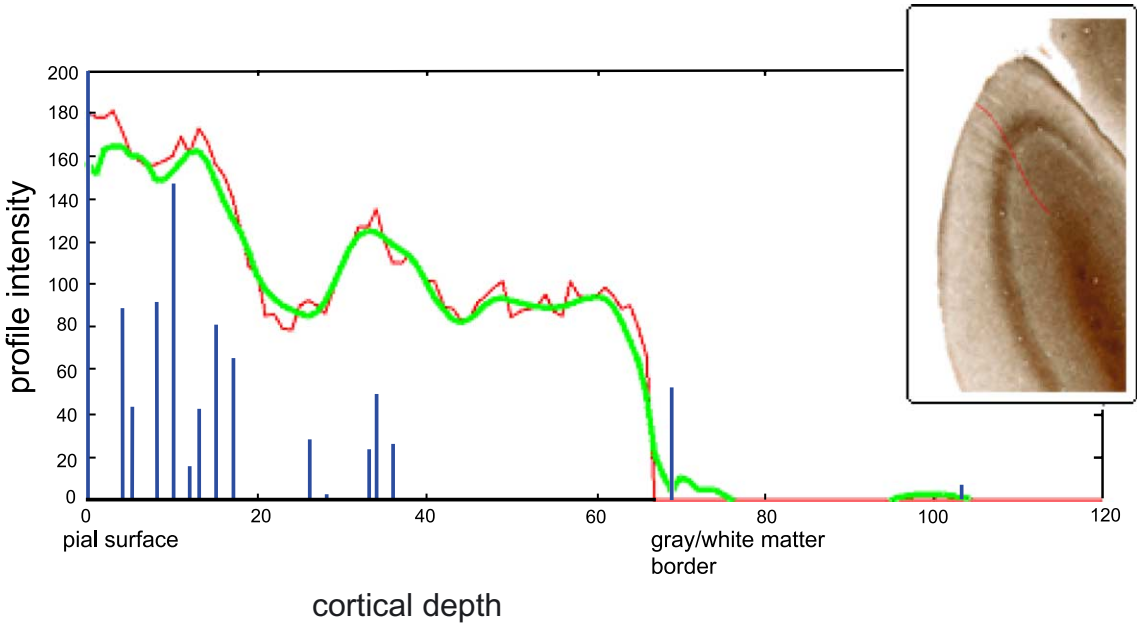

Fig. 3. The three curves on this graph represent the original signal (i.e., the cortical profile, red curve), its wavelet transform (blue curve) and the reconstructed function estimator using only the largest 5% of the wavelet parameters.

As a result, they define a layered set of nested contours that create a smooth transition from the pial surface to the cortex–white matter border and that are ideal for the computation of the cortical profiles (see Fig. 2).

From the delineated contours, we then obtain a profile array that corresponds to a flattening of the delimited cortical area.

Note that where the cortical region is very highly curved, the set of profiles computed from every pixel along the pial contour in the rasterized histological image does not span all the pixels inside the ribbon in concave areas. Conversely, considering every pixel along the gray–white matter contour would raise a similar concern in outer convex areas. This is essentially a rasterization problem; in the continuous domain, the properties of the harmonic function guarantee full coverage of the cortical ribbon. In view of the potentially complex curvature signature of the cortical mantel, we chose to super-sample the input histological section image and to consider every pixel along the pial contour in a rasterized image twice the resolution of the input section. There are no general prescriptions for this super-sampling factor: the higher the super-sampling, the less "forgotten" pixels in the ribbon but also the more pixels that are considered multiple times in adjacent profiles. Thus, too high a factor might create a substantial number of almost identical profiles. Although this does not impair the classification, it unnecessarily slows it down. The super-sampling factor could ideally be matched to the curvature of the ribbon. However, additional experiments with a varying factor showed no improvement of the classification performances: in practice, super-sampling by two creates a sufficiently dense net of profiles to suit our classification purposes.

Wavelet analysis of cortical profiles

We chose wavelet analysis (Daubechies, 1988) to extract from the profile array a compact representation that is more amenable to classification. The wavelet transform is indeed particularly well suited for that purpose because it bundles the input signal in a few large wavelet coefficients, well localized in the time-frequency space. It also maps rather noisy data to a much better behaved signal.

The wavelet basis for cortical profile curves is generated from an oscillatory, compactly supported, C^k differentiable wave function (ψ), which has rapidly decaying tails and satisfies an admissibility condition (Daubechies, 1988). Integral translations and scales of ψ, $\psi_{j,k} = 2^{j/2}\psi(2^{-j} - k)$ form an orthonormal basis for the space of cortical profile functions. Integrating the cortical signal against the base functions $\psi_{j,k}$ generates the corresponding spatial (index k) and frequency (index j) wavelet representation.

We use Dinov and Sumners (2001) wavelet shrinkage (frequency adaptive wavelet thresholding) approach to select the most significant wavelet coefficients computed for each profile (see Fig. 3). From each profile P_i in the cortical ribbon ($i = 1 \ldots N$), we then extract p wavelet coefficients

$$W_i = \begin{bmatrix} W_i^1 \\ \vdots \\ W_i^p \end{bmatrix}.$$

To take into account the location of the profiles (their spatial proximity), we add to the p wavelet coefficients the x,y coordinates of the starting point of the profile (along the pial contours) in the lattice.

W_i then writes

$$\begin{bmatrix} W_i^1 \\ \vdots \\ W_i^p \\ x_i \\ y_i \end{bmatrix}.$$

Architectonic classification of the cortical ribbon

We approach the issue of cortical segmentation as a process of partitioning the matrix of wavelet coefficients $W = [W_1, \ldots, W_N]$ associated with the profile array. We are looking for a hierarchical clustering of W, that is, a sequence of partitions in which each partition is nested into the next partition in the sequence.

Cluster analysis (unsupervised learning) essentially consists of sorting a series of multidimensional points (here a series of vectors $\{W_i\}_i$) into several groups (clusters) so as to maximize the intra-cluster versus the intercluster degree of association. It is particularly useful in this context as it behaves adequately even when very little is known about the category structure of the input set of points.

Clusters present the following relevant characteristics (see Everitt, 1974, for details):

- they are composed of several profiles which are 'similar' (with respect to a measure of similarity or distance) to each other, and dyssimilar to profiles from the other clusters.
- the distance between any two profiles in a given cluster is inferior to the distance between any profile of that cluster and any other profile in any other cluster.
- clusters can be represented by a densely populated connected region in a multidimensional space separated from the other dense regions by a relatively empty space.

To cluster W, we first need to compute a distance matrix $M = [m_{i,j}]$, where $i = 1 \ldots N$ and $j = 1 \ldots N$, which summarizes the "proximity" or similarity of any two sets of wavelet coefficients of W (i.e., the proximity of any two profiles):

$$\forall (i,j), m_{i,j} = \mathrm{dist}(W_i, W_j).$$

Given that the wavelet coefficients are decorrelated, we use a standardized Euclidean distance to assess the range and the variance differences between profiles:

$$\forall (i,j), \mathrm{dist}(W_i, W_j)^2 = [(W_j^1 - W_i^1) \ldots (W_j^p - W_i^p)(x_j - x_i) \quad (y_j - y_i)].V^{-1}. \begin{bmatrix} (W_j^1 - W_i^1) \\ \vdots \\ (W_j^p - W_i^p) \\ (x_j - x_i) \\ (y_j - y_i) \end{bmatrix}$$

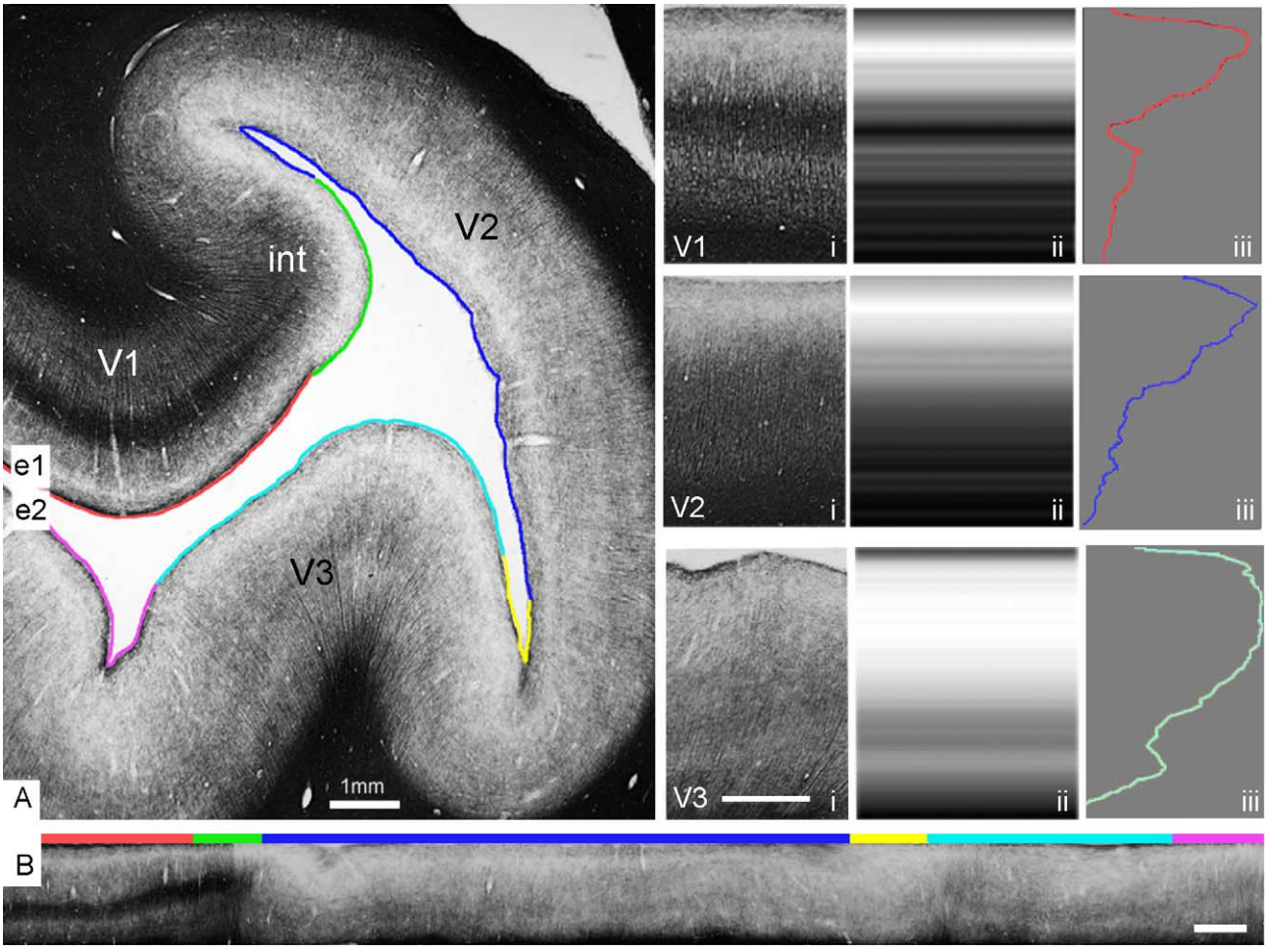

Fig. 4. (A) Myelo-architectonic classification results for the cortical sample displayed in Fig. 1. The clusters are projected with different colors from the starting point (e1) to the ending point (e2) of the external reference contour. The intermediate field (int) between V1 and V2 corresponds architectonically to area *Gb* of Sanides and Vitzhum (1965a,b). The transitional area between V2 and area V3 was classified as a separate sulcal field in view of its extreme tangential organization (in yellow; see text for an explanation). The original architecture of the tissue (i) is represented by the grayscale template (ii) that is, in turn, computed from the reparametrization and average of profiles belonging to independent clusters (iii). (B) The cortical ribbon is effectively straightened by the alignment of intensity profiles that were calculated via the Laplace equation. Scale bars = 1 mm.

where V = diag [Var(W^1),..., Var(W^p), Var(x), Var(y)] is the diagonal matrix of the variances of the first p wavelet coefficients and of the profile positions across the profile array.

Our cluster algorithm is the standard agglomerative hierarchical cluster method described in (Johnson, 1967), with single link:

Step 1. Start by placing each item of W in an individual cluster (disjoint cluster), and let the distance between any two of those clusters be the distance between the items they contain.

Step 2. Find the closest pair of clusters and merge them into a single cluster.

Step 3. Recompute the distance matrix: the distance between the newly formed cluster and any other cluster is the shortest distance from any member of the former to any member of the latter (single link).

Fig. 5. Classification and localization of *myelo*-architectonic fields in nine samples of human parietal and occipital cortex. Panels A and D contain samples from horizontal sections, all other panels show cortical samples from coronal sections. The classified clusters are mapped on the external reference contours in a congruent color-coded progressive order from starting point (e1) to the end point (e2) of the original tracings. Panel A displays the parcellation of three main visual areas (V1, V2 and V3) and a transitional field (*Gb*). These areas are homologous to the fields classified in Fig. 4. Panel H illustrates a case in which the same cluster, localized on the crown of the gyrus, is separated by an intermediate 'sulcal' field (in yellow). In the same panel, it is shown how the automatic classification disregarded a local variation created by tangential cut (T). In panel I, subfields *a* and *b* are segregated into different clusters but they represent the same architectonic field, as indicated by the distance matrix provided in Table 1. In both panels E and G, the parcellation of fields color coded in blue and green, respectively, seems to derive from the mean density of myelination. Ca = calcarine sulcus; cs = collateral sulcus; ios = inferior occipital sulcus; ips = intraparietal sulcus; los = lateral occipital sulcus; pos parieto-occipital sulcus; IV = fourth ventricle; AG = angular gyrus; FG = fusiform gyrus; MO/MT = transition between middle occipital and middle temporal gyri; MT = middle temporal gyrus; IT = inferior temporal gyrus; ST = superior temporal gyrus. The scale bar in panel H is valid for the other panels in figure.

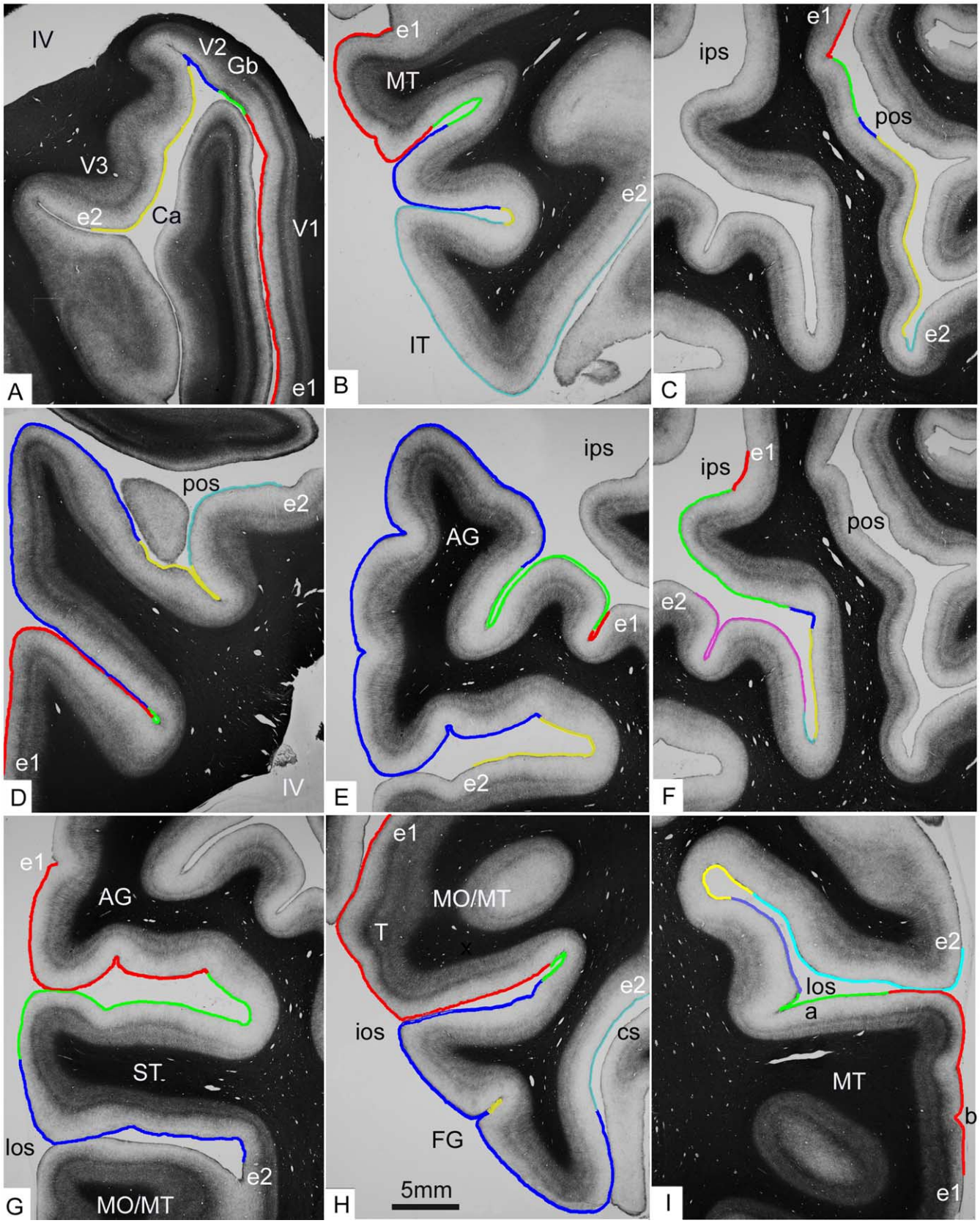
IV
V2
Gb
V3
e2
Ca
V1
e1
A
e1
MT
e2
IT
B
ips
e1
pos
e2
C
pos
e2
e1
IV
D
ips
AG
e1
e2
E
ips
e1
pos
e2
F
e1
AG
ST.
los
e2
MO/MT
G
e1
MO/MT
T
x
e2
ios
cs
FG
5mm
H
e2
los
a
MT
b
e1
I

Step 4: Repeat steps 2 and 3 until the desired number of clusters is obtained.

Profile arrays belonging to clusters segregated by the classification are averaged to produce a template representing a specific architechtonic field. We used the dynamic programming approach of Sebastian et al. (2000) with the observed transport measure of Pitiot et al. (2003) to match the intensity profiles in a curvature-dependent way. This reparameterization is necessary because the thickness of the cortex varies even within architectonic boundaries, and therefore the *absolute* position of features of interest may not be the same across the profile array belonging to a given cluster. Gray-scale images were created from the average curves to provide a more intuitive representation of specific architectonic types in the cortical samples.

Results

Intensity profiles presented high-frequency fluctuations due to the texture of myelination in the original images. By smoothing individual profiles in the wavelet domain, we obtained a compact representation of the data where the signal was represented by only few significant coefficients that were well localized in the time-frequency domain. For example, in Fig. 3, only 5% of the coefficients were sufficient to reconstruct the original profile with good accuracy.

The border between the primary visual cortex (the striate cortex) and area V2 (Brodmann's area 18) was adequately identified, including an intermediate area characterized by an intense radial fiber pattern (see Figs. 1, 4A and 5A). This narrow region corresponds to the *limes paratriatus gigantopyramidalis* (OBγ) of von Economo and Koskinas (1925) and to area *Gb* of Sanides and Vitzhum (1965a,b). Fig. 4 also illustrates the parcellation and the averaged templates relative to three exemplar classes of profile arrays: the visual areas V1, V2 and V3. The line of Gennari in layer IVb of V1 is clearly visible in the original image (i) and in both averaged representations (ii and iii). Another feature that was preserved by the averaging algorithm and that evidently concurred to the classification of area V1 is the collection of fibers in the zonal layer (layer 1) of the striate cortex. Area V2 was mainly characterized by the scarcity of horizontal fiber bundles in layer 2 and in layer 5 and more generally, by a graded transition to stronger myelination from layer 3 towards the white matter. The averaged model relative to the V3 cluster displays a distinctive stripe corresponding to the inner stria of Baillarger and a denser myelination in layer 1 compared to its bordering area V2.

To assess the robustness of our methodology, we operated the automatic classification in selected regions of convoluted isocortex. The borders assessed by the automatic algorithm coincided with the locations selected by an expert (J.A.) where unambiguous architectonic transitions were observable (see Fig. 5). The algorithm did not create areal boundaries where the neuroanatomist found reason to suspect variations due only to curvature. For example, the tangential area (T) in Fig. 5H did not induce the automatic definition of a border. The adjacent fields *a* and *b* in Fig. 5I have been segregated into different clusters. However, their average standardized Euclidean distance is significantly smaller than that of the other fields in the image (sees Table 1). This relationship suggests that they should be considered as a single architectonic field.

Table 1
Average distances between pairs of clusters (color-coded architectonic fields) classified from the image in Fig. 5I

	Red	Green	Blue	Yellow	Cyan
Red	0	85	151	283	102
Green	85	0	130	270	135
Blue	151	130	0	304	127
Yellow	283	270	304	0	184
Cyan	102	135	127	184	0

Discussion

Cortical topology

We presented an automatic method to describe the structural topography of the cortex based on the density and disposition of myelinated fibers. It was clear from the start that the high degree of curvature of the mantle was a major obstacle to the characterization of local cortical architecture. To avoid this potential problem, there have been efforts to chart the entire cortical surface by orthogonal slices producing hundreds of blocks sampled ad hoc in regions where the surface of the gyri was straight or 'fairly' straight (Vogt and Vogt, 1919). In our method, the problem of curvature is circumvented by the application of differential geometry (the classic heat conduction equation) by which it is possible to represent automatically the relationship between the curvature of the surface and the internal structure of the cortex as was done manually in previous studies (Smart and McSherry, 1986b; Van Essen and Maunsell, 1980). Our principal aim was to compute traverses that were generally perpendicular to the lamination of the cortex in order to minimize ambiguities in the classification of the intensity profiles. The solution of the second-order partial differential equation from the two reference contours (the perimeter of the meningeal surface and the boundary between gray and white matter) produced a series of nested contours that were geometrically consistent with the surface and coincident with cortical layers. It should be noted that, occasionally, the equipotential field lines did not follow the pattern of lamination precisely. Such errors occurred in areas where the cortex was cut tangentially to a certain extent (which means one or more layers were misrepresented); they reflect the limitation of applying this method to 2-D histological sections. A complete coincidence of cortical lamination with isopotential lines would allow the measure of intensity values along (and not across) cortical layers thereby demonstrating modular patterns that are distributed in specific levels of the cortex (e.g., the myelin-rich modules in layer III of the primary visual cortex).

The radial structure of the cortical volume is made quite evident, during development, by the course of glial fibers that guide neuronal migration (Rakic, 1988). At a later stage of maturation, it is possible to identify radially oriented dendrites that originate from spindle and pyramidal cells distributed through the depth of the cortex. A second population of radial fibers are the efferent and afferent subcortical projections. Other authors (Smart and McSherry, 1986b) used these features as built-in gauges to model internal structural changes induced by the expansion of the cortex. Their method was based on the topological procedure that

Nieuwenhuys (1972, 1974) applied to the comparative topographic study of the brainstem. What is significant about this approach is that the natural topology of a complex biological structure is respected. Our application of differential geometry represents a mathematical formalization of the approach of Smart and McSherry (1986b), and the vertical lines that are computed automatically follow the path of radial fibers that are stained by the silver impregnation technique.

In a very recent article, Schmitt and Böhme (2002) independently proposed a similar electrodynamic model to generate cortical profiles for the purpose of quantitative cyto-architectonic analysis. Straight lines were generated orthogonal to the external and innermost contours and not necessarily perpendicular to the intracortical layers. Whether or not, in highly curved portions of the cortex, the traverses cut across vertical tissue components was not important given that, at the magnification used, their Nissl-stained material did not resolve the vertical (i.e., modular) arrangement of the cortex. In contrast, myelin stain makes the radial architecture of the cortex extremely relevant to the classification. The fact that in our method the intensity profiles do not intersect radial fiber bundles greatly reduces noise levels and errors in the classification.

Maintaining fixed boundary conditions between the pial and inner boundaries of the cortex implies that in regions of strong curvature (convexity or concavity), the profile lines will be grouped together disproportionately (as noted in Fig. 2A, traverses are sparser at the crown of the gyri compared to the sulcal floor). This effect is inevitable as the two reference contours have different lengths. Results might be improved by switching boundary conditions where curvature is significant. Curvature could be computed automatically (Schmitt and Böhme, 2002) or coded manually while tracing the reference contours. Approaching the issue from an anatomical, rather than from computational perspective, it should be mentioned that the distinctive morphology of the sulcal floors and gyral crowns in the convoluted cortical mantle reflects specialized developmental and functional phenomena (Smart and McSherry, 1986b). While the former are dominated by horizontal cortico-cortical connective fibers, the latter display predominantly radial fibers the densest of which originate in subcortical nuclei. Sharp areal borders do not tend to occur in these regions, although the sulcal cortex is itself often a transitional field between areas. In this respect, the sampling effect abovementioned compromises the classification of cortical fields to a lesser extent.

Because of the amount of axonal fibers that perforate the deeper layers of the cortex, it is difficult to define a real border with the medullary substance. In fact, the analysis of the profiles did not reveal any obvious change in intensities at that level. The width of this ‘zona incerta’ of myelination varied from one region of the cortex to another. This finding introduces the problem in drawing a definite line of demarcation between the cortex and the white matter. Baillarger (1840; Article II, p. 155) had explicitly brought attention to this phenomenon stating that a simple juxtaposition of gray and white matter was not a tenable assumption. This is particularly true at the crown of cortical gyri, whereas in the fundus of the sulci, the cortex shows a predominant tangential organization creating a more evident borderline with the white matter system. This aspect of cortical anatomy is disquieting in the context of morphometric analyses that depend on the segmentation of gray and white matter in magnetic resonance images, where partial volume effects and lower resolution do not afford a clear definition of the tissue. For the purpose of analyzing intracortical profiles in histological sections, we traced the inner reference contour in the white matter respecting the curvature of the last visible lamina.

Myelo-architectonics

The nomenclature applied to myelo-architectonic types in the human cortex has the potential of becoming bewildering in view of the extremely variable combinations in which myelinated fibers can be arranged (Hopf, 1968; Sanides, 1972). To avoid confusion, we designed our method to extract the most significant components that play a determining role in the classification. For example, the classification of the primary visual cortex (V1) and hence the automatic determination of its boundaries was defined by very few parameters. This simplification, however, did not obscure anatomically significant features. A distinctively prominent zonal layer (layer 1) that is composed of a dense tangential plexus of delicate fibers was automatically detected as a further element for the classification of V1 (the striate cortex) versus its adjacent area V2 (see Figs. 4 and 5A). This feature may reflect the significance of extrastriate feedback connections in V1 (Rockland, 1997) and how the architectonic method may provide insight into the functional architecture of the cortex.

In the semiautomated cyto-architectonic parcellation proposed by Schleicher et al. (2000), the characterization of cortical profiles was based on the computation of feature vectors for which they assumed normal distribution. Profile similarity was then assessed using the usual Euclidean distance or normalized Mahalanobis distance between the standardized descriptor vectors. In contrast, we make no assumption about the distribution of the parameters in our descriptor vectors (the significant wavelet coefficients), avoiding the need to formulate any such hypothesis a priori.

We reported the automatic detection of a narrow intermediate field (i) between the striate cortex (V1) and area V2 (Figs. 4 and 5A). It corresponds topographically to a small projection area that is known to contain radially oriented callosal fibers (Clarke and Miklossy, 1990; Van Essen and Zeki, 1978). In addition to this border field Sanides and Vitzhum (1965a,b) described the transitory appearance (2–3 mm) of the inner stria of Baillarger at the fringe of area 17 and named this region *RS* (see also Lungwitz, 1937 and Sanides, 1972). Functionally, both border regions correspond to the representation of the vertical meridian of the visual field (Sereno et al., 1995). The second boundary feature *RS* was not evident in the material that we have examined, a discrepancy that could be explained in terms of differences in staining quality and the use of a different histotechnique. It is also possible that certain architectonic transitions appear different if the cortex is cut at different angles and in regions of different curvature. Further studies are necessary to verify myelo-architectonic parcellations using multiple staining protocols and to test the relationship of myelo-architectonic patterns to the curvature of the mantle.

The automated algorithm may sometimes segregate two architectonic clusters that are very similar (see Fig. 5I and Table 1). To localize such limit cases, we examine the average distance (average standardized Euclidean distance) between any two clusters provided by the classification. An explicit representation of the distance between clusters is useful for the interpretation of the results from the automatic classification and to define architectonic homologies, in a single image, across images and throughout the series of sections.

In view of the possible complexity of the category structure of the input profile data, there are no general prescriptions for selecting a suitable number of clusters. Although some preindicators—like the Davies–Bouldin index (Davies and Bouldin, 1979), for instance, or the cophenetic correlation coefficient (Backer, 1995)— can be used to assist this choice, they often suffer from strong outlier sensitivity. We are face with a circular problem which even more acutely affects the choice of a distance measure for the proximity matrix: namely, the quality of the cluster analysis (and thus of the choice of a distance measure and of several clusters) can only be assessed after the clusters have been formed. Assuming that the wavelet decomposition handles the dimension reduction issue in a satisfactory fashion, we are then left with two a priori hypotheses: the first on the nature of the cortical area transitions, which is linked to the choice of a distance measure; the second on the number of transitions we expect in a given cortical ribbon, which tells us how many clusters to look for. Our empirical studies suggest that the standardized Euclidean distance is adequate to recover inter-area transitions. We believe that the choice of the number of clusters depends on the goal of the study at hand. To pinpoint known transitions in an observer-independent way, an expert neuroanatomist may provide the number of clusters. Conversely, when trying to discover new transitions (new areas), the use of an independent index (cophenetic correlation coefficient for instance) seems more appropriate. Incidentally, the tendency of single-link hierarchical clustering techniques to rapidly (at low levels) cluster points linked by chains of intermediates (so-called ''chaining'' defect) increases its ability to group together patches of profiles (as opposed to profiles scattered all over the cortical ribbon) and thus plays in our favor.

The overall density of staining (i.e., the mean intensity in the image) may vary locally along the cortical ribbon. This architectonic parameter is not easily decomposed into discrete elements but seems to be correlated mainly with the number and diameter of vertical fibers. However, the level of nonspecific background staining may also affect this measure. A classification based on mean staining density alone would almost certainly be erroneous. In our method, mean intensity values of the profiles contribute to distinct wavelet coefficients that are used in cohort with other significantly large wavelet parameters. This implies that the mean density of staining of a cortical region is a factor that influences the classification without necessarily overruling it. This effect of wavelet decomposition is biologically relevant because while the absolute local staining intensity is obviously a meaningful parameter for classification, potential differences in staining conditions or illumination may produce artefactual intensity values that could bias the classification.

Nevertheless, architectonic classification remains subordinate to the outcome of histological methods used to resolve anatomical images. In this respect, it should be noted that different protocols that can be used to stain myelin may produce variable and even incongruent results. Horton and Hocking (1997) obtained idiosyncratic staining patterns from different techniques applied to flat preparations of the monkey cortex. Secondly, one single technique may yield qualitatively variable results. These may be due to the morbid condition of the specimen or to inconsistencies in the fixation and staining procedures. Because it is easy to demonstrate that by varying the duration of sensitive steps of histological protocols the picture of intracortical architecture may be changed dramatically, the comparison of the classification results across different subjects must be based on consistent and well-documented staining methods.

The effects of maturation and aging on the histological structure of the cortex must also be considered. According to Kemper (1994), age-dependent loss of myelination would be related to the length of the myelination cycle of a particular cortical region. By this principle, primary myelogenetic areas (numbered 1–10 in Flechsig's map of, 1920) maintain higher densities of staining than regions whose myelination depends on long association and commissural fibers. These fiber systems account for the main vertical component of intracortical myelination and exhibit most dramatic changes with development and aging. These changes would be reflected mainly in the mean density of staining. However, horizontal lamination may also change in homologous areas at different stages of maturation. For example, according to Yakovlev and Lecours (1967), the lamina of Kaes–Betchterew in the supragranular layers (see Fig. 1) is not really visible until the fourth decade of life. In the visual cortex, Lintl and Braak (1983) showed that the amount of myelin in the line of Gennari decreases after the third decade of life. Review of these studies indicates that efforts to compare myelo-architectonic data across subjects must be carefully controlled for the age of the donors.

In the context of present-day preliminary results in MR Microscopy of the human brain both in vivo (Burgess et al., 1999; Clark et al., 1992; Walters et al., 2003) and post-mortem (Barbier et al., 2002; Beuls et al., 1993; Fatterpekar et al., 2002; Kruggel, 2001), a meaningful myelo-architectonic classification should provide structural templates of the sort presented in Fig. 4 that can be used for validation and for structural characterization. It is to be expected that myelin will be an important indicator for in vivo architectonic cortical parcellations. Indeed, images that are emerging from the first generation of MRI 'architectonic scans' yield the level of detail contained in the original illustrations of Baillarger (1840) and Elliot Smith (1907). Eventually, new sequences and new hardware will provide sufficient resolution to resolve finer architectonic images. We expect that specific MR sequences will be run routinely before functional studies or diagnostic scans to obtain a map of cortical areas based on myelo-architecture. The method presented in this communication is readily exported in 3-D for the direct analysis of such microstructural tomographic data in brain mapping.

Acknowledgments

This work was supported by research grants from the National Library of Medicine (5 R01 LM05639), the NIH–National Center for Research Resources (P41 RR13642) and the NIH–National Institute of Mental Health (P20 MH65166 and P01 MH52176). J.A. wishes to thank Dr. Michael S. Gazzaniga (Center for Cognitive Neuroscience, Dartmouth College) and Dr. William F. Hickey (Department of Pathology, Dartmouth Medical School) for their scientific and academic support. A.P. was also supported by the INRIA associated team grant between EPIDAURE and LONI.

References

Annese, J., Toga, W.A., 2002. Postmortem anatomy. In: Toga, A.W., Mazziotta, J.C. (Eds.), Brain Mapping: The Methods, Second ed. Academic Press, New York, pp. 537–571.

Backer, E., 1995. Computer-Assisted Reasoning in Cluster Analysis. Prentice-Hall.

Baillarger, J., 1840. Recherces sur la structure de la couche corticale des circonvolutions du cerveau. Mém. Acad. R. Méd. 8, 149–183.

Barbier, E.L., Marrett, S., Danek, A., Vortmeyer, A., van Gelderen, P., Duyn, J., Bandettini, P., Grafman, J., Koretsky, A.P., 2002. Imaging cortical anatomy by high-resolution MR at 3.0T: detection of the stripe of Gennari in visual area 17. Magn. Reson. Med. 48 (4), 735–738.

Beuls, E., Gelan, J., Vandersteen, M., Adriaensens, P., Vanormelingen, L., Palmers, Y., 1993. Microanatomy of the excised human spinal cord and the cervicomedullary junction examined with high-resolution MR imaging at 9.4 Tesla. Am. J. Neuroradiol. 14 (3), 699–707.

Bevan-Lewis, W., 1878. On the comparative structure of the cortex cerebri. Brain 1, 79–86.

Bok, S.T., 1959. Histonomy of the Cerebral Cortex. Elsevier, Amsterdam.

Brodmann, K., 1909. Vergleichende Localisationslehre der Grosshirnrinde in ihren Prinzipien dargestellt auf Grund des Zellebaus. Barth, Leipzig.

Burgess, R.E., Yu, Y., Christoforidis, G.A., Bourekas, E.C., Chakeres, D.W., Spigos, D., Kangarlu, A., Abduljalil, A.M., Robitaille, P.M., 1999. Human leptomeningeal and cortical vascular anatomy of the cerebral cortex at 8 Tesla. J. Comput. Assist. Tomogr. 23 (6), 850–856.

Campbell, A.W., 1905. Histological Studies on the Localisation of Cerebral Function. Cambridge Univ. Press, Cambridge.

Clark, V.P., Courchesne, E., Grafe, M., 1992. In vivo myeloarchitectonic analysis of human striate and extrastriate cortex using magnetic resonance imaging. Cereb. Cortex 2 (5), 417–424.

Clarke, S., Miklossy, J., 1990. Occipital cortex in man: organization of callosal connections, related myelo- and cytoarchitecture, and putative boundaries of functional visual areas. J. Comp. Neurol. 298 (2), 188–214.

Daubechies, I., 1988. Orthonormal bases of compactly supported wavelets. Commun. Pure Appl. Math. 41, 909–996.

Davies, D.L., Bouldin, D.W., 1979. A cluster separation measure. IEEE Trans. Pattern Anal. Mach. Intell. 1, 224–227.

Dinov, I.D., Sumners, D.W.L., 2001. Applications of frequency dependent wavelet shrinkage to analyzing quality of image registration. SIAM J. Appl. Math. (SIAP) 62 (2), 367–384.

Elliot Smith, G., 1907. A new topographical survey of the human cerebral cortex, being an account of the anatomically distinct cortical areas and their relationship to the cerebral sulci. J. Anat. 41, 237–254.

Everitt, B.S., 1974. Cluster Analysis. Heinemann, London.

Fatterpekar, G.M., Naidich, T.P., et al., 2002. Cytoarchitecture of the human cerebral cortex: MR microscopy of excised specimens at 9.4 Tesla. Am. J. Neuroradiol. 23 (8), 1313–1321.

Flechsig, P., 1920. Anatomie des menschichen Gehirns und Ruckenmarks auf Myelogenetischer Grundlage. Thieme, Leipzig.

Gallyas, F., 1979. Silver staining of myelin by means of physical development. Neurol. Res. 1 (2), 203–209.

Gennari, F., 1782. De Peculiari Structura Cerebri. Nonnullisque ejus morbis. Ex Regio Typographeo, Parma.

Hopf, A., 1965. Objektive Registrierung der Myeloarchitektonic der Hirnrinde. Naturwissenschaften 52 (16), 479.

Hopf, A., 1968. Registration of the myeloarchitecture of the human frontal lobe with an extinction method. J. Hirnforsch. 10, 259–269.

Horton, J.C., Hocking, D.R., 1997. Myelin patterns in V1 and V2 of normal and monocularly enucleated monkeys. Cereb. Cortex 7 (2), 166–177.

Johnson, S.C., 1967. Hierarchical clustering schemes. Psychometrika 2, 241–254.

Jones, S.E., Buchbinder, B.R., et al., 2000. Three-dimensional mapping of cortical thickness using Laplace's equation. Hum. Brain Mapp. 11 (1), 12–32.

Kemper, L.T., 1994. Neuroanatomical and neuropathological changes during aging and dementia. In: Albert, L.M., Knoefel, E.J. (Eds.), Clinical Neurology of Aging, Second ed. Oxford Univ. Press, Oxford, pp. 3–67.

Kruggel, F., 2001. Analyzing the neocortical fine-structure. In: Insana, M.F., Leahy, R.M. (Eds.), Lecture Notes in Computer Science (IPMI 2001). Springer-Verlag, Berlin.

Lintl, P., Braak, H., 1983. Loss of intracortical myelinated fibers: a distinctive age-related alteration in the human striate area. Acta Neuropathol. (Berl.) 61 (3–4), 178–182.

Lungwitz, W., 1937. Zur myeloarchitektonischen Untergliederung der menschlichen Area praeoccipitalis (Area 19 Brodmann). J. Psychol. Neurol. 47, 607–638.

Meynert, T., 1872. In: Stricker, S. (Ed.), Vom Gehirn der Saugethiere. Handbuch der Lehere von den Geweben des Menshen. Engelmann, Leipzig, pp. 694–808.

Nieuwenhuys, R., 1972. Topological analysis of the brain stem of the lamprey *Lampetra fluviatilis*. J. Comp. Neurol. 145 (2), 165–177.

Nieuwenhuys, R., 1974. Topological analysis of the brain stem: a general introduction. J. Comp. Neurol. 156 (3), 255–276.

Pitiot, A., Delingette, H., Toga, A.W., Thompson, P.M., 2003. Learning shape correspondences with the observed transport shape measure. Information Processing in Medical Imaging (IPMI '03).

Rakic, P., 1988. Specification of cerebral cortical areas. Science 241, 170–176.

Rockland, K.S., 1997. Elements of cortical architecture. In: Rockland, K.S., Kaas, J.H., Peters, A. (Eds.), Extrastriate Cortex in Primates. Cerebral Cortex, vol. 12. Plenum, New York, pp. 243–287.

Roland, P.E., Geyer, S., et al., 1997. Cytoarchitectural maps of the human brain in standard anatomical space. Hum. Brain Mapp. 5, 222–227.

Sanides, F., 1972. Representation in the cerebral cortex and its areal lamination patterns. In: Bourne, G.F. (Ed.), Structure and Function of Nervous Tissue, vol. 5. Academic Press, New York, pp. 329–453.

Sanides, F., Vitzhum, H.G., 1965a. Die Grenzerscheinungen am Rande der menschlichen Sehrinde. Dtsch. Z. Nervenheilkd. 187, 708–719.

Sanides, F., Vitzhum, H.G., 1965b. Zur Architektonik der menschlichen Sehrinde und den Prinzipien ihrer Entwicklung.

Schleicher, A., et al., 1999. Observer-independent method for microstructural parcellation of cerebral cortex: a quantitative approach to cytoarchitectonics. NeuroImage 9 (1), 165–177.

Schleicher, A., et al., 2000. A stereological approach to human cortical architecture: identification and delineation of cortical areas. J. Chem. Neuroanat. 20 (1), 31–47.

Schmitt, O., Böhme, M., 2002. A robust transcortical profile scanner for generating 2-d traverses in histological sections of richly curved cortical courses. NeuroImage 16 (4), 1103–1119.

Sebastian, T.B., Crisco, J.J., Klein, P.N., Kimia, B.B., 2000. Constructing 2D curve atlases. Proceeding of CVPR Computer Vision and Pattern Recognition. IEEE Computer Society, pp. 70–77.

Sereno, M.I., Dale, A.M., Reppas, J.B., Kwong, K.K., Belliveau, J.W., Brady, T.J., Rosen, B.R., Tootell, R.B., 1995. Borders of multiple visual areas in humans revealed by functional magnetic resonance imaging. Science 268 (5212), 889–893.

Smart, I.H., McSherry, G.M., 1986a. Gyrus formation in the cerebral cortex in the ferret: I. Description of the external changes. J. Anat. 146, 141–152.

Smart, I.H., McSherry, G.M., 1986b. Gyrus formation in the cerebral cortex of the ferret: II. Description of the internal histological changes. J. Anat. 147, 27–43.

Van Essen, D.C., Maunsell, J.H., 1980. Two-dimensional maps of the cerebral cortex. J. Comp. Neurol. 191 (2), 255–281.

Van Essen, D.C., Zeki, S.M., 1978. The topographic organization of rhesus monkey prestriate cortex. J. Physiol. 277, 193–226.

Vicq d'Azyr, F., 1786. Traite d'anatomie et de physiologie. F.A. Didot, Paris.

Vogt, O., 1910. Die Myeloarchitektonische Felderung des des menschlichen stirnhirns. J. Psychol. Neurol. 15, 221–238.

Vogt, C., Vogt, O., 1919. Allgemeinere ergbnisse unserer Hirnforschung. J. Psychol. Neurol. 25, 399–462.

von Economo, C., Koskinas, G.N., 1925. Die Cytoarchitectonik der Hirnrinde des erwachsenen Menschen. Springer, Vienna.

Walters, N.B., Egan, G.F., Kril, J.J., Kean, M., Waley, P., Jenkinson, M., Watson, J.D., 2003. Proc. Natl. Acad. Sci. U. S. A. 100 (5), 2981–2986.

Yakovlev, P.I., Lecours, A.R., 1967. The cycles of myelogenetic cycles of regional maturation of the brain. In: Minkowski, A. (Ed.), Regional development of the Brain in Early Life. Blackwell Scientific Publications, Oxford, pp. 3–65.

Zilles, K., Schleicher, A., 1993. Cyto- and myeloarchitecture of human visual cortex and the periodical GABAA receptor distribution. In: Gulyas, B., et al. (Eds.), Functional Organisation of the Human Visual Cortex. Pergamon, Oxford, pp. 111–122.

Zilles, K., et al., 2002. In: Toga, A.W., Mazziotta, J.C. (Eds.), Quantitative Analysis of Cyto- and Receptor Architecture of the Human Brain. Brain Mapping: the Methods, Second ed. Academic Press, New York, pp. 573–602.